ACS APPLIED OPTICAL MATERIALS

pubs.acs.org/acsaom

Article

Antimony-Doped Tin Oxide Hole Injection Interlayer Improving the Efficiency of Perovskite Nanocrystal Light Emitting Diodes

A. Ioakeimidis, F. Galatopoulos, M. Athanasiou, A. Hauser, M. Rossier, M. I. Bodnarchuk, M. V. Kovalenko, G. Itskos, and S. A. Choulis*

Cite This: *ACS Appl. Opt. Mater.* 2024, 2, 528−534

Read Online

ACCESS | Metrics & More | Article Recommendations | Supporting Information

ABSTRACT: We present significant performance enhancement of $CsPbBr_3$ perovskite nanocrystal (NC) light emitting diodes (PNC LEDs) by incorporation of a solution processed doped metal oxide hole injection interlayer consisting of 10 atom % doped antimony tin oxide (ATO) within the PNC LEDs device architecture. The incorporation of an ATO interlayer between ITO and poly-TPD improves the bottom electrode hole injection properties and provides charge balanced PNC LEDs that show three and half times increased luminance, lower turn-on voltage, and improved maximum current and power efficiency compared to reference $CsPbBr_3$ PNC LEDs incorporating the commonly used PEDOT:PSS hole injection interlayer.

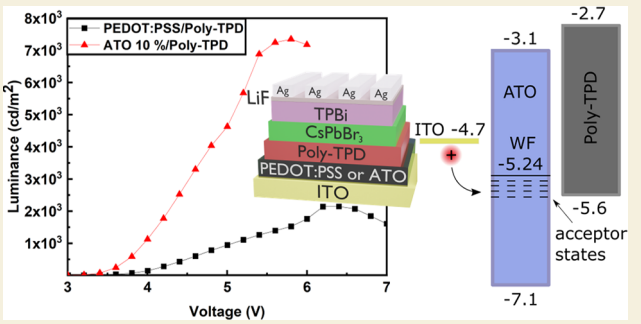

KEYWORDS: *Perovskite nanocrystal light emitting diodes, Doped metal oxides, Hole injection layers, Interfaces, Charge balanced, Electrodes*

1. INTRODUCTION

Perovskite nanocrystals (PNCs) have risen to prominence over the last years as strong candidates for optoelectronic applications.[1−5] Compared to 3D bulk perovskites, PNCs show superior phase stability (e.g., for $CsPbBr_3$ and $FAPbI_3$) as well as easier processing as colloidal inks.[6−8] The main rule that PNCs abide by is the reduction of at least one dimension in order to satisfy the condition of quantum confinement effect.[9]

PNCs exhibit important properties due to their low dimensionality that are attractive for optoelectronic applications and especially for next generation LEDs applications. Some of these properties include narrow emission bandwidth, defect tolerance, high photoluminescence quantum yield (PLQY), and high band gap tunability by varying the nanocrystal (NC) size.[10−13] Traditionally, 3D perovskites have low exciton binding energy which leads to dissociation and promotion of nonradiative recombination, which is unfavorable for LED applications.[14,15] On the other hand, PNCs due quantum confinement exhibit much higher exciton binding energy which promotes radiative recombination, a property that is highly desirable for luminescent devices such as LEDs.[16,17] Furthermore, ionic defect density is reduced in PNCs compared to 3D bulk perovskites due to the processing conditions that result in better crystallinity, therefore further reducing the nonradiative recombination pathways.[18−20] These properties have led to significant improvements for perovskite nanocrystal light emitting diodes (PNC LEDs) with an EQE > 20% over the last years for green-, red-, and near-infrared (IR)-based NCs.[21−23]

Apart from the properties of the PNC active layer, the electrode properties are equally important for the development of high-performance PNC LEDs. The PNC active layer is "sandwiched" between a hole injection layer (HIL) and an electron injection layer (EIL) in PNC LEDs. Efficient charge injection layers (CIL) are considered those that are highly conductive and selective on the majority carrier (holes for HIL and electrons for EIL) as well as resistive for the minority carriers (electrons for HIL and holes for EIL).[24] An equally important property of the electrodes is the provision of balanced charge injection. Imbalance in charge injection can lead to the accumulation of carriers at the interfaces and exciton quenching that limits the efficiency of PNC LEDs. Buffer layer engineering is a common strategy to improve the electrode properties of the device. Interlayers such as polyvinylpyrrolidone (PVP) and polyethylamine have been incorporated between ZnO and the PNC active layer providing better charge balance and improved energy level alignment.[25,26] Furthermore, poly(methyl methacrylate) (PMMA)

Received: January 26, 2024
Revised: February 23, 2024
Accepted: March 5, 2024
Published: March 14, 2024

has also been utilized to further optimize the charge balance by restraining the injection of excess electrons in electron dominated devices.[27,28] Apart from retarding the electron injection, improving the hole injection is also an efficient strategy to improve carrier balance in electron dominated devices. The hole injection contact of PNC LEDs usually consists of PEDOT:PSS HIL combined with hole transporting layers (HTLs). Nevertheless, the low mobility of the common HTLs (e.g., PVK, PTAA) compared to ETLs as well as the mismatch of their highest occupied molecular orbital (HOMO) with PEDOT:PSS HIL causes an imbalance distribution of opposite charges in the active layer that can deteriorate the device performance. Lu et al. compared the use of TFB, PTAA, and PVK as HTLs in $CsPbBr_3$-based PNC LEDs, concluding that PTAA provides devices with lower turn-on voltage and higher luminance (1054 cd/m^2) ascribed to a lower energetic barrier (0.1 eV) between PEDOT:PSS and PTAA.[29] To reduce this energetic barrier Xiao et al. introduced a ultrathin thermally evaporated MoO_3 between PEDOT:PSS and PVK to form an interfacial dipole and improve hole injection in a $FAPb_{0.7}Sn_{0.3}Br_3$-based device resulting in enhanced higher luminance and current efficiency.[30] Hu et al. implemented a double interlayer concept consisting of TFB/PVK that provided enhanced current efficiency and external quantum efficiency for $FAPb_{0.7}Sn_{0.3}Br_3$-based PNC LEDs compared to single TFB or PVK interlayer based devices.[31] In another work, Li et al. introduced a thermally evaporated ultrathin (2 nm) LiF between the PEDOT:PSS and the $MAPbBr_3$ emissive layer. The LiF layer reduced the roughness, passivated the interface defects, and provided more balanced charge injection that resulted in improved maximum luminance (6713.9 cd/m^2) and reduced turn-on voltage (3.8 V).[32] The aforementioned method is a successful methodology for enhancing the performance of solution-processed PNC LEDs; however, the controlled incorporation of an ultrathin layer demands a thermal evaporation step that increases the complexity of the fabrication process of solution-processed PNC LEDs.

In this paper, we show that by introducing doped metal oxide HIL within the device architecture the electro-optical PNC LEDs performance is significantly improved compared to devices employing the commonly used PEDOT:PSS HIL. Importantly the proposed doped metal oxide HIL is solution processed and thus is introduced within the PNC LEDs device architecture with a facile fabrication at ambient and room temperature conditions. Spray pyrolysis 10 atom % antimony-doped tin oxide (ATO) is a solution processed commercially available nanoparticulated p-type doped metal-oxide semiconductor provided by AVANTAMA AG [product number, (ATO, 10095)] with a relatively high electrical conductivity (10^{-3} S/cm). More details on the synthesis and materials properties of ATO can be found elsewhere.[33] ATO has been previously successfully applied as buffer layer in normal and inverted device architecture organic photovoltaics (OPVs)[34,35] and the development of silver nanowire (AgNW)-based electrodes for the fabrication of highly efficient ITO-free inverted OPVs.[36]

As discussed also above, PNC LEDs usually incorporated PEDOT:PSS as HIL. In this report, the commonly used PEDOT:PSS is replaced with a solution-processed ATO HIL for green $CsPbBr_3$ PNC LEDs using the following device architecture: glass/ITO/HIL/poly-TPD/$CsPbr_3$/TBPi/LiF/Ag. Importantly, the 30 nm solution-processed ATO interlayer was fabricated in air using a doctor blade without any further treatment simplifying the fabrication process and importantly circumventing the thermal annealing step requirement for processing PEDOT:PSS HILs. The ATO HIL-based PNC LEDs provide three and half times increased luminance, lower turn-on voltage, and improved maximum current and power efficiency compared to PEDOT:PSS HIL-based PNC LEDs. The presented measurements on hole-only devices and impedance spectroscopy-based capacitance−frequency (C-f) results reveal that the performance enhancement of ATO-based $CsPbBr_3$ PNC LEDs is due to increased hole injection properties that provide charge balanced PNC LEDs. The origin of the improved hole injection is due to a reduced hole injection energetic barrier that lowers the bottom electrode contact resistance for the corresponding PNC LEDs incorporating the proposed ATO HIL within their device architecture.

2. MATERIALS AND METHODS

Materials

Prepatterned glass-ITO substrates (sheet resistance 4Ω sq^{-1}) were purchased from Psiotec Ltd. Poly(*N*,*N*′-bis-4-butylphenyl-*N*,*N*′-bisphenyl)benzidine (poly-TPD (52kD)) and PEDOT:PSS (PVP Al) were purchased from Ossila Ltd. $CsPbBr_3$ NCs capped with didodecyldimethylammonium bromide (DDAB) were synthesized following the procedure described in a previous report.[37] 2,2′,2″-(1,3,5-Benzinetriyl)-tris(1-phenyl-1-H-benzimidazole) (TPBi) was purchased from Merck KGaA. The commercially available antimony-doped tin oxide (10 at% Sb:SnO_2) solution in mixture of butanols was developed by Avantama (ATO, Product-No. 10095). Lithium fluoride (LiF) pieces (99.9%) and silver (Ag) pellets (99.99%) were purchased from Kurt J. Lesker Company.

Device Fabrication

ITO substrates were sequentially sonicated in acetone and isopropanol for 10 min and were air blown to remove the remaining solvents. Before, PEDOT:PSS deposition the substrates were treated with UV−O_3 for 20 min. The PEDOT:PSS was spin-coated on top of the ITO at 4000 rpm for 30 s in air and annealed at 140 °C for 20 min resulting in ∼30 nm thickness. The ATO was blade coated in air without any further treatment. Then, poly-TPD was spin coated on PEDOT:PSS and ATO at 4000 rpm in air for 60 s without any further treatment from a 6 mg/mL chlorobenzene solution. The $CsPbBr_3$ NCs layer was spin-coated at 6000 rpm for 60 s without any further treatment from an 18 mg/mL solution in toluene. Next, 40 nm TPBi and 1 nm LiF were sequentially thermally evaporated at 0.1 Å/s. Finally, 100 nm Ag layers were thermally evaporated through a shadow mask to complete the devices (active area of 9 mm^2). The measurements of the resulting devices were performed under ambient conditions without encapsulation.

Single-Carrier Devices

Hole-only device (HODs) configuration is ITO/HIL/poly-TPD/$CsPbBr_3$ /MoO_3/Ag, following the same processing steps and materials as described above. The MoO_3 HIL and Ag electrode were thermally evaporated to form 10 nm (0.2 Å/s) and 100 nm (2 Å/s) thick layers, respectively.

Characterization

The thickness of the films was measured with a Veeco Dektak 150 profilometer. Current density−voltage−luminance characteristics (JVL) of the devices were obtained using a Botest LIV Functionality Test System with a calibrated silicon photodiode sensor (spectral sensitivity of 350−730 nm and responsivity of 60 nA/lux). AFM images were obtained by using a Nanosurf easy scan 2 controller under the tapping mode. The optical transmittance and absorbance measurements were performed with a Schimadzu UV-2700 UV−vis optical spectrophotometer. Steady-state PL measurements were

https://doi.org/10.1021/acsaom.4c00044
ACS Appl. Opt. Mater. 2024, 2, 528−534

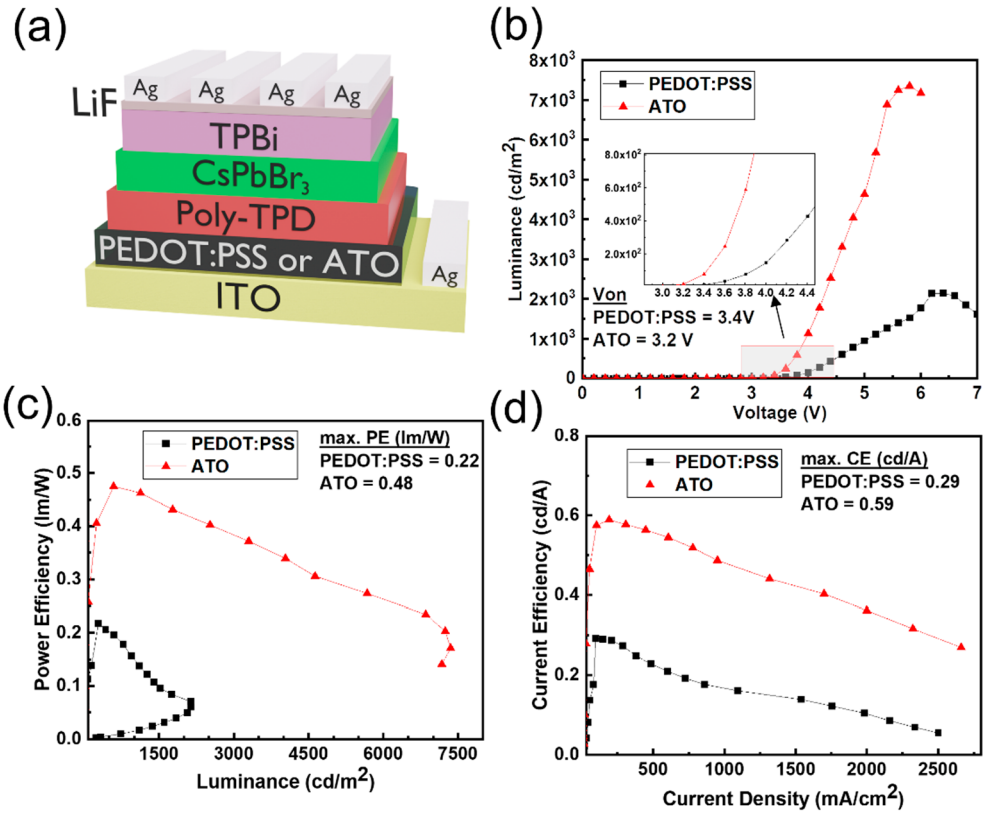

Figure 1. (a) Device structure of green PNC LEDs ($CsPbBr_3$) with PEDOT:PSS or ATO as hole injection layer and (b) luminance, (c) power efficiency, and (d) current efficiency of the respective PNC LEDs.

performed on an FP-8300 Jasco spectrometer. Capacitance−frequency (EIS) measurements were obtained using a Metrohm Autolab PGSTAT 302N instrument applying a small AC perturbation of 20 mV and a DC bias of 4 V.

3. RESULTS AND DISCUSSION

The device architecture of the $CsPbBr_3$-based PNC LEDs under study is glass/ITO (150 nm)/HIL/poly-TPD(~40 nm)/$CsPbBr_3$/TBPi(40 nm)/LiF(1 nm)/Ag (100 nm) as illustrated in Figure 1(a). Two solution processed electronic materials were implemented as HIL: the ~30 nm commonly used PEDOT:PSS(PVP Al) is designated as the reference device of the study, and the ~30 nm ATO which is proposed as an alternative HIL for PNC LEDs within this paper. In the above device architecture, the layers of HIL/poly-TPD serve as the hole injection/electron blocking layer, and the layers of TBPi/LiF serve as the electron injection/hole blocking layer. The luminance−voltage curves of each PNC LEDs are presented in Figure 1(b). ATO HIL-based PNC LEDs show much higher luminance of almost three and half times (7350 cd/m^2) at 5.8 V compared to PEDOT:PSS HIL-based PNC LEDs which exhibited a luminance of 2115 cd/m^2 at 6.4 V. Concurrently, the turn-on voltage (V_{on}, defined at 10 cd/m^2) of ATO HIL-based PNC LEDs is reduced to 3.2 V compared to 3.4 V for PEDOT:PSS HIL-based PNC LEDs. The calculated maximum power efficiency PE_{max} (Figure 1(c)) and current efficiency CE_{max} (Figure 1(d)) are enhanced for the ATO HIL-based PNC LEDs compared to those of PEDOT:PSS HIL-based PNC LEDs. Specifically, the ATO HIL-based PNC LEDs reaches its higher PE_{max} of 0.48 lm/W at 587 cd/m^2 while at the peak of its luminance (7350 cd/m^2) exhibits a PE of 0.17 lm/W. The PEDOT:PSS-based PNC LEDs provide a much lower PE_{max} of 0.22 lm/W at 282 cd/m^2 and at the peak of its luminance (2115 cd/m^2) exhibiting a PE of only 0.07 lm/W. Similarly, the CE_{max} for the ATO HIL-based PNC LEDs is 0.59 cd/A at 191 mA/cm^2 current density, which is higher than the PEDOT:PSS HIL-based PNC LEDs that yield a value of 0.25 cd/A at 96.4 mA/cm^2 current density. Figure S1 demonstrates the statistical distribution of the luminance values obtained from 28 different devices using either ATO or PEDOT:PSS as HIL in the $CsPbBr_3$-based PNC LEDs, and Figure S2 demonstrates the statistical distribution of luminance for ATO thicknesses 30, 45, and 55 nm.

To get a better understanding of the improved performance of the ATO HIL-based PNC LEDs device, further characterization studies were performed. Figure S3 shows the absorbance and photoluminance (PL) of the $CsPbBr_3$ NCs emissive layer processed on a glass substrate, where a characteristic band edge absorption close to 500 nm is observed for the UV−vis measurement. The PL peak center is at 516 nm with a Gaussian fwhm of ~20 nm. Contact angle measurements (Figure S4) showed the good wetting properties of chlorobenzene/poly-TPD on both PEDOT:PSS and ATO underlayer exhibiting contact angles of 7.3° and 5.4°, respectively. Figure 2(a, b) shows the surface topography using AFM images of the $CsPbBr_3$ NC emissive layer spin-casted on top of poly-TPD for PEDOT:PSS and ATO underlayers, respectively. The roughness (RMS) of the PNC emissive layer on the top of PEDOT:PSS/poly-TPD underlayers was calculated to be 4.5 nm, which is lower compared to the respective value for the PNC emissive layer fabricated on the top of ATO/poly-TPD that calculated to be 10.1 nm. The higher roughness of the $CsPbBr_3$ NC emissive layer on the top

https://doi.org/10.1021/acsaom.4c00044
ACS Appl. Opt. Mater. 2024, 2, 528−534

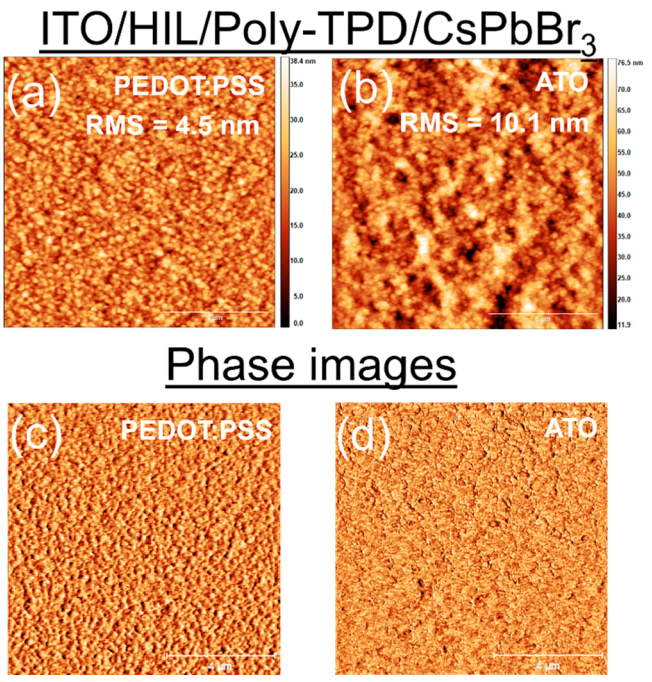

Figure 2. AFM images (10 μm × 10 μm) and the calculated roughness (RMS) of the $CsPbBr_3$ films fabricated on top of poly-TPD using (a) PEDOT:PSS or (b) ATO as underlayer. Panels (c) and (d) present the corresponding phase images.

of the ATO/poly-TPD underlayers is the result of the nanoparticulate metal oxide nature of ATO which induces higher roughness to the upper processed layers of poly-TPD (Figure S5) and $CsPbBr_3$, respectively. $CsPbBr_3$ NCs on the top of PEDOT:PSS/poly-TPD underlayers form a compact, pinhole-free PNC emissive layer. Despite the higher roughness of $CsPbBr_3$ NCs on the top of ATO/poly-TPD underlayers, the solution processed $CsPbBr_3$ NCs also form a compact, pinhole-free PNC emissive layer as can be derived from the smooth phase images obtained by the AFM images [Figure 2(c, d)].

Optical transmittance measurements were performed to evaluate the impact of each layer stacking transparency on the luminance. Figure 3(a) presents the transmission of glass/ITO/HIL/poly-TPD for PEDOT:PSS and ATO HILs, respectively. At the emission wavelength region (516 nm) of $CsPbBr_3$ NC, the transmission level of both PEDOT:PSS/poly-TPD and ATO/poly-TPD underlayers is similar, and thus, the optical transparency of the underlayers under study has no effect on the luminance difference of the $CsPbBr_3$ PNC LEDs incorporating the respective underlayers.

Electrical characterization by current density−voltage (J-V) measurements were performed on single carrier PNC LED device architectures in which electron injection is intentionally blocked [hole-only devices (HOD)]. For the fabrication of hole-only devices, the TPBi/LiF/Ag electron injection electrode was replaced by the thermally evaporated hole injection layer MoO_3(10 nm)/Ag (100 nm). Figure 3(b) presents the J-V characteristics of the PNC LEDs incorporat-

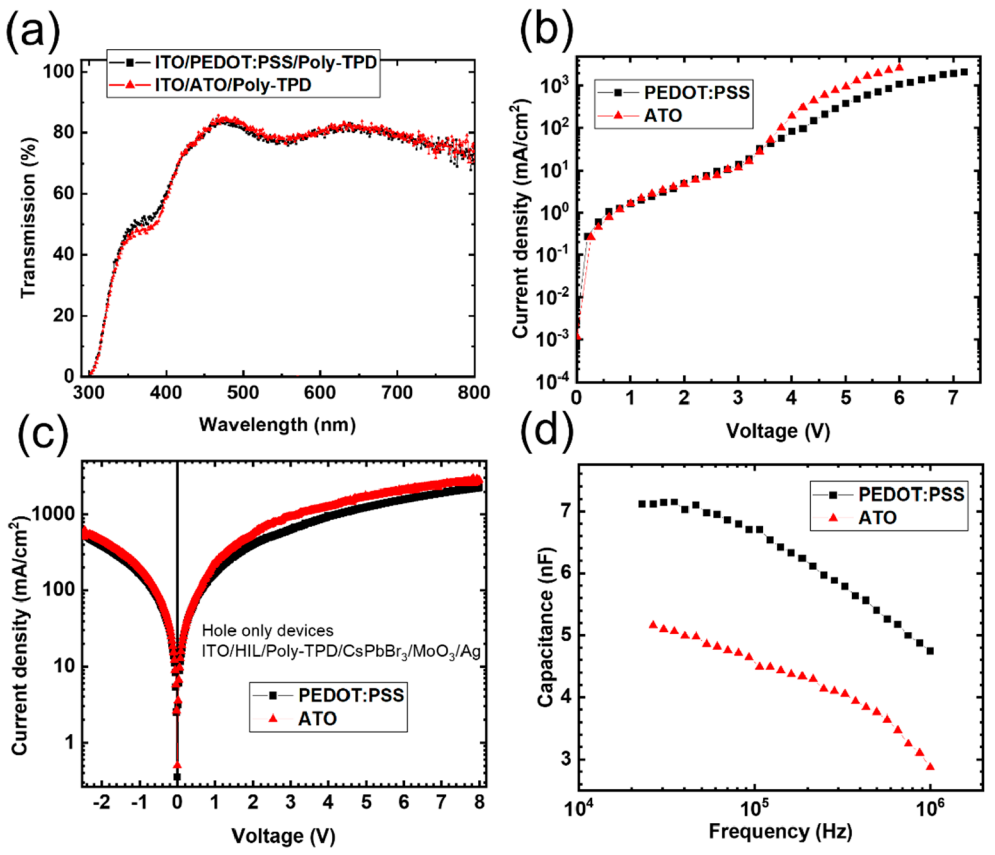

Figure 3. (a) Optical transmittance of ITO/PEDOT:PSS or ATO/poly-TPD. Current density−voltage (J-V) curves of the theee (b) PNC LED devices and three (c) hole-only devices (HOD) incorporating as HIL PEDOT:PSS or ATO. (d) Capacitance−frequency (C-f) curves of the respective PNC LED devices incorporating PEDOT:PSS and ATO, respectively.

https://doi.org/10.1021/acsaom.4c00044
ACS Appl. Opt. Mater. 2024, 2, 528−534

ing PEDOT:PSS and ATO HILs, respectively. At the ohmic region of the forward biased devices, the current densities are similar, while at the working region (higher biases) the current density for the ATO HIL-based PNC LEDs surpasses the PEDOT:PSS HIL-based PNC LEDs. The HOD incorporating ATO HIL exhibits enhanced current density (Figure 3(c)) compared to PEDOT:PSS HIL-based HOD. Since the electrical conductivity of PEDOT:PSS and ATO are similar, in the order of 10^{-3} S/cm,[32] the experimental results of HODs indicate that the hole injection properties of the ITO/ATO/poly-TPD bottom electrode for the $CsPbr_3$ PNC LEDs are improved.

The higher current density for the ATO HIL compared to PEDOT:PSS HIL devices at higher bias is consistent with the enhanced luminance at the working bias region of the PNC LEDs incorporating ATO HIL. Also considering the improved CE of the PNC LEDs incorporating ATO HIL compared to that obtained by the corresponding PNC LEDs incorporating PEDOT:PSS HIL shown in Figure 1(d), it is inferred that ATO HIL provides more balanced transport of the opposite charges carriers (suppressing the space charge buildup at the ATO/poly-TPD interface) in the emissive layer compared to the PEDOT:PSS/poly-TPD interface. To further support our findings, the impedance response of $CsPbBr_3$ PNC LEDs with ATO and PEDOT:PSS HILs is also investigated. Figure 3(d) shows the capacitance−frequency measurements of the corresponding $CsPbBr_3$ PNC LEDs performed under a 4 V bias. Indeed, the PEDOT:PSS HIL-based $CsPbBr_3$ PNC LED exhibits a higher capacitance at higher frequencies compared to ATO HIL-based $CsPbBr_3$ PNC LED. The lower capacitance for the ATO HIL-based PNC LEDs is attributed to lower charge densities present in the ATO HIL-based $CsPbBr_3$ PNC LEDs due to more frequent charge recombination/emission achieved by the incorporation of the proposed ATO HIL within the PNC LEDs device architecture that provides improved charge balance $CsPbBr_3$ PNC LEDs.

According to the reported experimentally verified energy levels for the presented ATO, the antimony (Sb) doping of SnO_2 introduces deep acceptor states in the band gap (deeper than intrinsic Fermi level) converting the SnO_2 from an n-type to a p-type semiconductor.[34] Thus, due to the unique ATO properties, even though the valence band minimum (VBM) of ATO is much deeper than the poly-TPD the ATO acceptor states in the band gap[33] almost perfectly align with the VBM of the poly-TPD inducing a lower contact resistance (lower energetic barrier) for improved hole injection and lower turn-on voltage (V_{on}) for the ATO HIL-based PNC LEDs as shown above. The improved hole injection process by the incorporation of ATO HIL within the $CsPbBr_3$ LEDs structure is depicted in Figure 4 using a simplified band energy level diagram with energy values adopted from advanced characterization studies from the literature.[34,38,39] Thus, by lowering the energetic barrier between the ATO/poly-TPD the space charge buildup is suppressed compared to PEDOT:PSS/poly-TPD improving the effective mobility of holes in the ATO-based PNC LEDs. As a result, a higher number of holes can reach the emissive layer within an arbitrary time interval (higher current density), balancing the electron−hole pairs within the emissive layer, yielding improved luminance and current efficiency.

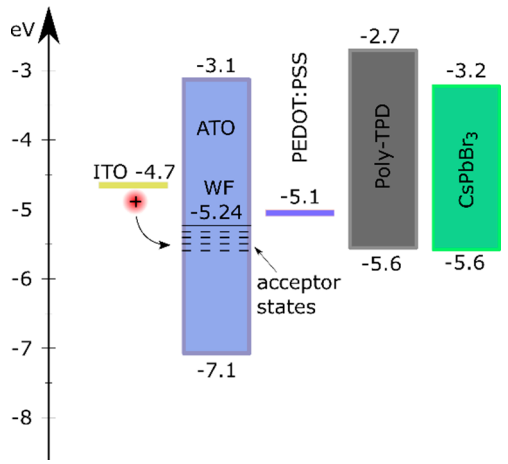

Figure 4. Simplified energy level depiction of ITO/ATO or PEDOT:PSS/poly-TPD/$CsPbBr_3$ of the PNC LEDs device structure, where the acceptor states (dashed lines) induced by Sb doping of SnO_2 contribute to efficient bottom electrode hole injection resulting in enhanced performing $CsPbBr_3$ PNC LEDs.

4. CONCLUSIONS

The effect of the appropriate solution-processed doped metal oxide interlayer between ITO and poly-TPD on the performance of PNC LEDs is demonstrated. Improved hole injection properties were achieved by incorporating ATO HIL between ITO and poly-TPD. The device architecture of the $CsPbBr_3$-based perovskite LEDs under study is glass/ITO/HIL/poly-TPD/$CsPbBr_3$/TBPi/LiF/Ag. Two different electronic materials were implemented as HILs: the commonly used PEDOT:PSS is designated as reference HIL of the study and the new proposed ATO HIL. Importantly, the 10 atom % doped ATO-based $CsPbBr_3$ PNC LEDs exhibit almost three and half times higher luminance compared to PEDOT:PSS-based PNC LEDs and lower turn-on voltage. Furthermore, the calculated maximum power efficiency PE_{max} and current efficiency CE_{max} are enhanced for the ATO HIL-based NC PE LEDs compared to those of PEDOT:PSS HIL PNC LEDs. Thus, this paper provides a novel bottom electrode interface engineering strategy that achieved significant efficiency enhancement of PNC LEDs. The enhanced performance is attributed to the improved hole injection properties of the ATO-based bottom electrode, which consequently provided better charge balance for the $CsPbBr_3$ PNC LEDs.

■ ASSOCIATED CONTENT

Supporting Information

The Supporting Information is available free of charge at https://pubs.acs.org/doi/10.1021/acsaom.4c00044.

Figure S1: Statistical distribution of luminance obtained from 28 different CsPbBr3-based PNC LEDs using either ATO or PEDOT:PSS as hole injection layer. Figure S2: Statistical distribution of luminance obtained for ATO-based CsPbBr3 PNC LEDs using 30, 45, and 55 nm thick ATO hole injection layer. Figure S3: Absorbance and photoluminance of CsPbBr3 NCs emissive layer. Figure S4: Contact angle of poly-TPD/chlorobenzene solution on PEDOT:PSS and ATO underlayers. Figure S5: AFM images (10 μm × 10 μm) and calculated roughness (RMS) of poly-TPD fabricated on top of PEDOT:PSS and ATO (PDF)

https://doi.org/10.1021/acsaom.4c00044
ACS Appl. Opt. Mater. 2024, 2, 528−534

AUTHOR INFORMATION

Corresponding Author

S. A. Choulis − *Molecular Electronics and Photonics Research Unit, Department of Mechanical Engineering and Materials Science and Engineering, Cyprus University of Technology, Limassol 3603, Cyprus;* orcid.org/0000-0002-7899-6296; Email: stelios.choulis@cut.ac.cy

Authors

A. Ioakeimidis − *Molecular Electronics and Photonics Research Unit, Department of Mechanical Engineering and Materials Science and Engineering, Cyprus University of Technology, Limassol 3603, Cyprus;* orcid.org/0000-0003-3974-6574

F. Galatopoulos − *Molecular Electronics and Photonics Research Unit, Department of Mechanical Engineering and Materials Science and Engineering, Cyprus University of Technology, Limassol 3603, Cyprus*

M. Athanasiou − *Department of Physics, Experimental Condensed Matter Physics Laboratory, University of Cyprus, Nicosia 1678, Cyprus;* orcid.org/0000-0003-1684-9482

A. Hauser − *Avantama AG, Staefa 8712, Switzerland*

M. Rossier − *Avantama AG, Staefa 8712, Switzerland*

M. I. Bodnarchuk − *Laboratory for Thin Films and Photovoltaics, Empa − Swiss Federal Laboratories for Materials Science and Technology, CH-8600 Dübendorf, Switzerland;* orcid.org/0000-0001-6597-3266

M. V. Kovalenko − *Laboratory for Thin Films and Photovoltaics, Empa − Swiss Federal Laboratories for Materials Science and Technology, CH-8600 Dübendorf, Switzerland; Institute of Inorganic Chemistry, Department of Chemistry and Applied Biosciences, ETH Zürich, CH-8093 Zürich, Switzerland;* orcid.org/0000-0002-6396-8938

G. Itskos − *Department of Physics, Experimental Condensed Matter Physics Laboratory, University of Cyprus, Nicosia 1678, Cyprus*

Complete contact information is available at: https://pubs.acs.org/10.1021/acsaom.4c00044

Notes

The authors declare no competing financial interest.

ACKNOWLEDGMENTS

This work was financially supported by the Research and Innovation Foundation of Cyprus under the "NEW STRATEGIC INFRASTRUCTURE UNITS-YOUNG SCIENTISTS" Programme (Grant Agreement No. "INFRASTRUCTURES/1216/0004", Acronym "NANOSONICS"). We would like to thank Miss Caterina Bernasconi for providing valuable assistance on the synthesis of $CsPbBr_3$ perovskite nanocrystals and AVANTAMA AG for providing the latest batch of their commercially available antimony-doped tin oxide (ATO) [(product number, (ATO, 10095)] to complete the presented studies.

REFERENCES

(1) Kovalenko, M. V.; Protesescu, L.; Bodnarchuk, M. I. Properties and Potential Optoelectronic Applications of Lead Halide Perovskite Nanocrystals. *Science (80-.)* **2017**, *358* (6364), 745−750.

(2) Shamsi, J.; Urban, A. S.; Imran, M.; De Trizio, L.; Manna, L. Metal Halide Perovskite Nanocrystals: Synthesis, Post-Synthesis Modifications, and Their Optical Properties. *Chem. Rev.* **2019**, *119* (5), 3296−3348.

(3) Swarnkar, A.; Marshall, A. R.; Sanehira, E. M.; Chernomordik, B. D.; Moore, D. T.; Christians, J. A.; Chakrabarti, T.; Luther, J. M. Quantum Dot−Induced Phase Stabilization of α-CsPbI 3 Perovskite for High-Efficiency Photovoltaics. *Science (80-.).* **2016**, *354* (6308), 92−95.

(4) Huang, H.; Polavarapu, L.; Sichert, J. A.; Susha, A. S.; Urban, A. S.; Rogach, A. L. Colloidal Lead Halide Perovskite Nanocrystals: Synthesis, Optical Properties and Applications. *NPG Asia Mater.* **2016**, *8* (11), e328−e328.

(5) Dey, A.; Ye, J.; De, A.; Debroye, E.; Ha, S. K.; Bladt, E.; Kshirsagar, A. S.; Wang, Z.; Yin, J.; Wang, Y.; Quan, L. N.; Yan, F.; Gao, M.; Li, X.; Shamsi, J.; Debnath, T.; Cao, M.; Scheel, M. A.; Kumar, S.; Steele, J. A.; Gerhard, M.; Chouhan, L.; Xu, K.; Wu, X.; Li, Y.; Zhang, Y.; Dutta, A.; Han, C.; Vincon, I.; Rogach, A. L.; Nag, A.; Samanta, A.; Korgel, B. A.; Shih, C.-J.; Gamelin, D. R.; Son, D. H.; Zeng, H.; Zhong, H.; Sun, H.; Demir, H. V.; Scheblykin, I. G.; Mora-Seró, I.; Stolarczyk, J. K.; Zhang, J. Z.; Feldmann, J.; Hofkens, J.; Luther, J. M.; Pérez-Prieto, J.; Li, L.; Manna, L.; Bodnarchuk, M. I.; Kovalenko, M. V.; Roeffaers, M. B. J.; Pradhan, N.; Mohammed, O. F.; Bakr, O. M.; Yang, P.; Müller-Buschbaum, P.; Kamat, P. V.; Bao, Q.; Zhang, Q.; Krahne, R.; Galian, R. E.; Stranks, S. D.; Bals, S.; Biju, V.; Tisdale, W. A.; Yan, Y.; Hoye, R. L. Z.; Polavarapu, L. State of the Art and Prospects for Halide Perovskite Nanocrystals. *ACS Nano* **2021**, *15* (7), 10775−10981.

(6) Liu, L.; Najar, A.; Wang, K.; Du, M.; Liu, S. Perovskite Quantum Dots in Solar Cells. *Adv. Sci.* **2022**, *9* (7), No. 2104577.

(7) Yuan, J.; Ling, X.; Yang, D.; Li, F.; Zhou, S.; Shi, J.; Qian, Y.; Hu, J.; Sun, Y.; Yang, Y.; Gao, X.; Duhm, S.; Zhang, Q.; Ma, W. Band-Aligned Polymeric Hole Transport Materials for Extremely Low Energy Loss α-CsPbI3 Perovskite Nanocrystal Solar Cells. *Joule* **2018**, *2* (11), 2450−2463.

(8) Liu, C.; Zeng, Q.; Wei, H.; Yu, Y.; Zhao, Y.; Feng, T.; Yang, B. Metal Halide Perovskite Nanocrystal Solar Cells: Progress and Challenges. *Small Methods* **2020**, *4* (10), No. 2000419.

(9) Peng, X.; Yan, C.; Chun, F.; Li, W.; Fu, X.; Yang, W. A Review of Low-Dimensional Metal Halide Perovskites for Blue Light Emitting Diodes. *J. Alloys Compd.* **2021**, *883*, No. 160727.

(10) Xie, M.; Liu, H.; Chun, F.; Deng, W.; Luo, C.; Zhu, Z.; Yang, M.; Li, Y.; Li, W.; Yan, W.; Yang, W. Aqueous Phase Exfoliating Quasi-2D CsPbBr 3 Nanosheets with Ultrahigh Intrinsic Water Stability. *Small* **2019**, *15* (34), No. 1901994.

(11) Meggiolaro, D.; Motti, S. G.; Mosconi, E.; Barker, A. J.; Ball, J.; Andrea Riccardo Perini, C.; Deschler, F.; Petrozza, A.; De Angelis, F. Iodine Chemistry Determines the Defect Tolerance of Lead-Halide Perovskites. *Energy Environ. Sci.* **2018**, *11* (3), 702−713.

(12) Chun, F.; Zhang, B.; Li, Y.; Li, W.; Xie, M.; Peng, X.; Yan, C.; Chen, Z.; Zhang, H.; Yang, W. Internally-Externally Defects-Tailored MAPbI3 Perovskites with Highly Enhanced Air Stability and Quantum Yield. *Chem. Eng. J.* **2020**, *399*, No. 125715.

(13) Song, J.; Li, J.; Li, X.; Xu, L.; Dong, Y.; Zeng, H. Quantum Dot Light-Emitting Diodes Based on Inorganic Perovskite Cesium Lead Halides (CsPbX 3). *Adv. Mater.* **2015**, *27* (44), 7162−7167.

(14) Liu, X.-K.; Xu, W.; Bai, S.; Jin, Y.; Wang, J.; Friend, R. H.; Gao, F. Metal Halide Perovskites for Light-Emitting Diodes. *Nat. Mater.* **2021**, *20* (1), 10−21.

(15) Herz, L. M. Charge-Carrier Dynamics in Organic-Inorganic Metal Halide Perovskites. *Annu. Rev. Phys. Chem.* **2016**, *67* (1), 65−89.

(16) Kamminga, M. E.; Fang, H.-H.; Filip, M. R.; Giustino, F.; Baas, J.; Blake, G. R.; Loi, M. A.; Palstra, T. T. M. Confinement Effects in Low-Dimensional Lead Iodide Perovskite Hybrids. *Chem. Mater.* **2016**, *28* (13), 4554−4562.

(17) Gao, P.; Bin Mohd Yusoff, A. R.; Nazeeruddin, M. K. Dimensionality Engineering of Hybrid Halide Perovskite Light Absorbers. *Nat. Commun.* **2018**, *9* (1), 5028.

(18) Yang, Z.; Wang, M.; Qiu, H.; Yao, X.; Lao, X.; Xu, S.; Lin, Z.; Sun, L.; Shao, J. Engineering the Exciton Dissociation in Quantum-

Confined 2D CsPbBr 3 Nanosheet Films. *Adv. Funct. Mater.* **2018**, *28* (14), No. 1705908.
(19) Fu, Y.; Zhu, H.; Chen, J.; Hautzinger, M. P.; Zhu, X.-Y.; Jin, S. Metal Halide Perovskite Nanostructures for Optoelectronic Applications and the Study of Physical Properties. *Nat. Rev. Mater.* **2019**, *4* (3), 169−188.
(20) Hong, K.; Le, Q. V.; Kim, S. Y.; Jang, H. W. Low-Dimensional Halide Perovskites: Review and Issues. *J. Mater. Chem. C* **2018**, *6* (9), 2189−2209.
(21) Kim, Y.-H.; Kim, S.; Kakekhani, A.; Park, J.; Park, J.; Lee, Y.-H.; Xu, H.; Nagane, S.; Wexler, R. B.; Kim, D.-H.; Jo, S. H.; Martínez-Sarti, L.; Tan, P.; Sadhanala, A.; Park, G.-S.; Kim, Y.-W.; Hu, B.; Bolink, H. J.; Yoo, S.; Friend, R. H.; Rappe, A. M.; Lee, T.-W. Comprehensive Defect Suppression in Perovskite Nanocrystals for High-Efficiency Light-Emitting Diodes. *Nat. Photonics* **2021**, *15* (2), 148−155.
(22) Chiba, T.; Hayashi, Y.; Ebe, H.; Hoshi, K.; Sato, J.; Sato, S.; Pu, Y.-J.; Ohisa, S.; Kido, J. Anion-Exchange Red Perovskite Quantum Dots with Ammonium Iodine Salts for Highly Efficient Light-Emitting Devices. *Nat. Photonics* **2018**, *12* (11), 681−687.
(23) Xu, W.; Hu, Q.; Bai, S.; Bao, C.; Miao, Y.; Yuan, Z.; Borzda, T.; Barker, A. J.; Tyukalova, E.; Hu, Z.; Kawecki, M.; Wang, H.; Yan, Z.; Liu, X.; Shi, X.; Uvdal, K.; Fahlman, M.; Zhang, W.; Duchamp, M.; Liu, J.-M.; Petrozza, A.; Wang, J.; Liu, L.-M.; Huang, W.; Gao, F. Rational Molecular Passivation for High-Performance Perovskite Light-Emitting Diodes. *Nat. Photonics* **2019**, *13* (6), 418−424.
(24) Dyrvik, E. G.; Warby, J. H.; McCarthy, M. M.; Ramadan, A. J.; Zaininger, K.-A.; Lauritzen, A. E.; Mahesh, S.; Taylor, R. A.; Snaith, H. J. Reducing Nonradiative Losses in Perovskite LEDs through Atomic Layer Deposition of Al 2 O 3 on the Hole-Injection Contact. *ACS Nano* **2023**, *17* (4), 3289−3300.
(25) Zhang, L.; Yang, X.; Jiang, Q.; Wang, P.; Yin, Z.; Zhang, X.; Tan, H.; Yang, Y.; Wei, M.; Sutherland, B. R.; Sargent, E. H.; You, J. Ultra-Bright and Highly Efficient Inorganic Based Perovskite Light-Emitting Diodes. *Nat. Commun.* **2017**, *8* (1), No. 15640.
(26) Wang, N.; Cheng, L.; Ge, R.; Zhang, S.; Miao, Y.; Zou, W.; Yi, C.; Sun, Y.; Cao, Y.; Yang, R.; Wei, Y.; Guo, Q.; Ke, Y.; Yu, M.; Jin, Y.; Liu, Y.; Ding, Q.; Di, D.; Yang, L.; Xing, G.; Tian, H.; Jin, C.; Gao, F.; Friend, R. H.; Wang, J.; Huang, W. Perovskite Light-Emitting Diodes Based on Solution-Processed Self-Organized Multiple Quantum Wells. *Nat. Photonics* **2016**, *10* (11), 699−704.
(27) Lin, K.; Xing, J.; Quan, L. N.; de Arquer, F. P. G.; Gong, X.; Lu, J.; Xie, L.; Zhao, W.; Zhang, D.; Yan, C.; Li, W.; Liu, X.; Lu, Y.; Kirman, J.; Sargent, E. H.; Xiong, Q.; Wei, Z. Perovskite Light-Emitting Diodes with External Quantum Efficiency Exceeding 20 per Cent. *Nature* **2018**, *562* (7726), 245−248.
(28) Dai, X.; Zhang, Z.; Jin, Y.; Niu, Y.; Cao, H.; Liang, X.; Chen, L.; Wang, J.; Peng, X. Solution-Processed, High-Performance Light-Emitting Diodes Based on Quantum Dots. *Nature* **2014**, *515* (7525), 96−99.
(29) Lu, Y.; Wang, Z.; Chen, J.; Peng, Y.; Tang, X.; Liang, Z.; Qi, F.; Chen, W. Tuning Hole Transport Layers and Optimizing Perovskite Films Thickness for High Efficiency CsPbBr3 Nanocrystals Electroluminescence Light-Emitting Diodes. *J. Lumin.* **2021**, *234*, No. 117952.
(30) Xiao, X.; Wang, K.; Ye, T.; Cai, R.; Ren, Z.; Wu, D.; Qu, X.; Sun, J.; Ding, S.; Sun, X. W.; Choy, W. C. H. Enhanced Hole Injection Assisted by Electric Dipoles for Efficient Perovskite Light-Emitting Diodes. *Commun. Mater.* **2020**, *1* (1), 81.
(31) Hu, L.; Ye, Z.; Wu, D.; Wang, Z.; Wang, W.; Wang, K.; Cui, X.; Wang, N.; An, H.; Li, B.; Xiang, B.; Qiu, M. Marked Efficiency Improvement of FAPb0.7Sn0.3Br3 Perovskite Light-Emitting Diodes by Optimization of the Light-Emitting Layer and Hole-Transport Layer. *Nanomaterials* **2022**, *12* (9), No. 1454.
(32) Li, Z.; Cao, K.; Li, J.; Du, X.; Tang, Y.; Yu, B. Modification of Interface between PEDOT:PSS and Perovskite Film Inserting an Ultrathin LiF Layer for Enhancing Efficiency of Perovskite Light-Emitting Diodes. *Org. Electron.* **2020**, *81*, No. 105675.
(33) Georgiou, E.; Papadas, I. T.; Antoniou, I.; Oszajca, M. F.; Hartmeier, B.; Rossier, M.; Luechinger, N. A.; Choulis, S. A. Antimony Doped Tin Oxide/Polyethylenimine Electron Selective Contact for Reliable and Light Soaking-Free High Performance Inverted Organic Solar Cells. *APL Mater.* **2019**, *7* (9), No. 091103.
(34) Liu, C.; Félix, R.; Forberich, K.; Du, X.; Heumüller, T.; Matt, G. J.; Gu, E.; Wortmann, J.; Zhao, Y.; Cao, Y.; He, Y.; Ying, L.; Hauser, A.; Oszajca, M. F.; Hartmeier, B.; Rossier, M.; Lüchinger, N. A.; Liu, Y.; Guo, J.; Nie, K.; Wilks, R. G.; Bachmann, J.; Bär, M.; Li, N.; Brabec, C. J. Utilizing the Unique Charge Extraction Properties of Antimony Tin Oxide Nanoparticles for Efficient and Stable Organic Photovoltaics. *Nano Energy* **2021**, *89*, No. 106373.
(35) Ioakeimidis, A.; Hauser, A.; Rossier, M.; Linardi, F.; Choulis, S. A. High-Performance Non-Fullerene Acceptor Inverted Organic Photovoltaics Incorporating Solution Processed Doped Metal Oxide Hole Selective Contact. *Appl. Phys. Lett.* **2022**, *120* (23), 233301.
(36) Georgiou, E.; Ioakeimidis, A.; Antoniou, I.; Papadas, I. T.; Hauser, A.; Rossier, M.; Linardi, F.; Choulis, S. A. Non-Embedded Silver Nanowires/Antimony-Doped Tin Oxide/Polyethylenimine Transparent Electrode for Non-Fullerene Acceptor ITO-Free Inverted Organic Photovoltaics. *ACS Appl. Electron. Mater.* **2023**, *5*, 181.
(37) Bodnarchuk, M. I.; Boehme, S. C.; Ten Brinck, S.; Bernasconi, C.; Shynkarenko, Y.; Krieg, F.; Widmer, R.; Aeschlimann, B.; Günther, D.; Kovalenko, M. V.; Infante, I. Rationalizing and Controlling the Surface Structure and Electronic Passivation of Cesium Lead Halide Nanocrystals. *ACS Energy Lett.* **2019**, *4* (1), 63−74.
(38) Huang, C.-Y.; Chang, S.-P.; Ansay, A. G.; Wang, Z.-H.; Yang, C.-C. Ambient-Processed, Additive-Assisted CsPbBr3 Perovskite Light-Emitting Diodes with Colloidal NiOx Nanoparticles for Efficient Hole Transporting. *Coatings* **2020**, *10* (4), No. 336.
(39) Lee, C.; Kim, H.; Kim, Y. Short-Wave Infrared Organic Phototransistors with Strong Infrared-Absorbing Polytriarylamine by Electron-Transfer Doping. *npj Flex Electron.* **2021**, *5* (1), 1−9.

https://doi.org/10.1021/acsaom.4c00044
ACS Appl. Opt. Mater. 2024, 2, 528−534